Solar-Terrestrial Physics. 2026, vol. 12, iss. 2, pp. 21–33. DOI: 10.12737/stp-122202603. © 2026 N.V. Savelyeva, V.A. Pilipenko, O.I. Yagodkina. Published by INFRA-M Academic Publishing House

DOI: 10.12737/stp-122202603
EDN: VDKLYJ

Received August 16, 2025
Accepted December 22, 2025

WHICH LATITUDES OF THE RUSSIAN FEDERATION MAY BE AFFECTED BY EXTREME MAGNETIC STORMS?

N.V. Savelyeva
Schmidt Institute of Physics of the Earth RAS, Moscow, Russia, nasa2000@ya.ru
Geophysical Center RAS, Moscow, Russia

V.A. Pilipenko
Schmidt Institute of Physics of the Earth RAS, Moscow, Russia
Geophysical Center RAS, Moscow, Russia, pilipenko_va@mail.ru

O.I. Yagodkina
Polar Geophysical Institute KSC RAS, Apatity, Russia, yagodkina@pgia.ru

Abstract. If we consider the auroral oval as an indicator of the electrojet position, the information about the position of its equatorial boundary allows us to predict the latitudes at which the most intense geomagnetic variations can be observed. These variations are the source of geomagnetically induced currents (GICs), which pose a threat to the stable operation of electric power systems. The Starkov-93 (S93) model, Auroral Precipitation Model (APM), and OVATION Prime (OP) model are widely used to estimate the possible minimum latitude of the oval. However, the databases with the aid of which these models were built did not contain rare extreme magnetic storms (|*Dst*|>400 nT). As a source of information on auroral latitudes during extreme storms, we employ the statistical model of the minimum latitude of the equatorial boundary of discrete auroras L2025, which is based on observational evidence. Extrapolation of the dependences of the oval's equatorial boundary latitude on the storm intensity obtained by the S93 model and APM during extreme storms (|*Dst*|>400 nT) diverge from the predictions of the L2025 model. In the new version of APM (APM_GEO), the limits to the magnetic activity level in the *AL* and *Dst* indices were removed, which makes it possible to estimate the location of the precipitation boundary during super substorms and extreme storms. To compare the OP model with APM_GEO, we have examined the dynamics of the auroral oval during the May 10–11, 2024 magnetic storm and have constructed maps of the position of the oval equatorial boundaries for different storm phases for the territory of the Russian Federation. As revealed from the comparison with APM_GEO, the OP model driven by interplanetary medium parameters significantly underestimates latitudinal shift of the oval. Since intense substorms during storms lead to a significant equatorial shift of the oval boundary, all large energy grids of the Russian Federation can be affected by GICs not only during extreme, but also during strong magnetic storms in the presence of intense substorms against their background.

Keywords: space weather, magnetic storms, geomagnetically induced currents, auroral oval.

INTRODUCTION

Ironically, the more colorful and fascinating auroras are caused by magnetic storms, the more dangerous they are for satellite and ground technological systems. Strong storms activate relativistic electron fluxes in the radiation belt that disable satellite electronics [Effects of Space Weather..., 2004; Pilipenko et al., 2006], interfere with signals from global navigation satellite systems (GNSS) [Yasyukevich et al., 2013], distort results of inclinometric measurements during directional drilling of deep wells [Gvishiani, Lukyanova, 2018], cause overloads in electric power systems [Baker et al., 2008; Hapgood, 2012; Pilipenko, 2021], lead to failures in railway signaling [Pilipenko et al., 2023a, b], shorten the service life of pipeline transport [Kostarev et al., 2023].

The main source of ground geomagnetic disturbances are variations in the auroral electrojet, which generate geoelectric fields driving geomagnetically induced currents (GICs) in high-voltage power transmission lines (PTLs) [Boteler, 2003; Dimmock et al., 2019; Kozyreva et al., 2018]. The auroral electrojet is concentrated in the auroral oval [Feldstein et al., 1999; Walker et al., 2024]. Under quiet geomagnetic conditions, the nighttime equatorial boundary of the aurora oval is located in the geomagnetic latitude range to ~70°, but after the onset of a magnetic storm the oval expands and its equatorial boundary descends to lower latitudes. As the oval expands, the intensity of geomagnetic disturbances and the strength of GICs they excite increase at midlatitudes [Kataoka, Ngwira, 2016; Woodroffe et al., 2016].

The auroral oval is also a region with high ionospheric turbulence. This region features sharp ionospheric plasma gradients, which cause signal phase retardation and significantly decrease the stability of GNSS [Edemskiy, Yasyukevich, 2022]. During magnetic storms, the zone with unstable reception of GNSS signals expands considerably.

The auroral oval equatorial boundary latitude is one of the key parameters of space weather. The dynamics of the auroral oval during strong and extreme storms is usually closely related to the dynamics of the main magnetospheric structures. The location of the auroral oval is essential for an adequate description of the dynamics of Earth's outer radiation belt [Myagkova et al., 2010; Tverskaya, 2011]. The maximum in the latitudinal power distribution of ultra-low-frequency waves in the Pc5 range is bound to the equatorial boundary of the oval [Kozyreva et al., 2016]. In this regard, the cosmophysical community has been making a lot of efforts to build models that can predict the location of the auroral oval.

The first auroral oval models were based on ground-based photographic observations of auroras (Khoro-sheva, 1961; Feldstein, 1963). Despite the simplicity of such models, the model designed by Starkov [1993, 1994] (hereinafter S93) is still successfully used in space geophysics [Tverskaya, 2011]. Efforts were made to develop a model of the auroral oval from its UV emission recorded by highly elliptical orbit satellites [Carbary et al., 2003; Chisham et al., 2022], yet the period of such observations was short. It is possible to reconstruct the latitudinal profile of the auroral electrojet from ground-based geomagnetic data, but this requires a dense meridional network of stations [Johnsen, 2013; Evdokimova, Petrukovich, 2020]. Attempts are also made to build an auroral oval model based on data on field-aligned currents recorded by magnetometers of low-orbit satellites [Gary et al., 1998; Xiong et al., 2014].

One of the most reliable methods for determining auroral oval boundaries is to record charged particle fluxes by low-orbit satellites, which makes it possible to identify both ionospheric projections of boundary regions of the magnetosphere and the auroral oval itself. Using long-term data from the Defense Meteorological Satellite Program (DMSP) spacecraft, a statistical OVATION Prime (OP) model, parameterized by interplanetary data, was built [Sotirelis, Newell, 2000; Newell et al., 2014]. A similar model, parameterized by the geomagnetic indices *Dst* and *AL*, the Aurora Precipitation Model (APM, as well as its new version APM_GEO), was constructed at the Polar Geophysical Institute [Vorobjev et al., 2013; Vorobjev et al., 2023].

The observational databases used to develop the above models included strong magnetic storms with $|Dst|$~200 nT, but there were no extreme events during instrumental observations. It is, therefore, unknown whether these models can be extrapolated to the case of extreme magnetic storms with $|Dst|$>400 nT. In order to collect information about latitudes of auroras during extreme space weather events, Blake et al. [2021] and Love et al. [2025] have examined visual observations of auroras reported in the press. A list of the lowest latitudes at which discrete auroras were observed at the local zenith for each storm was compiled, and on its basis a statistical model (hereinafter L2025) of the auroral oval equatorial boundary latitude was constructed depending on storm intensity characterized by the *Dst* index. Despite the obvious limitations of this model, it allows at least a rough estimate of the location of the auroral oval boundary during extreme storms.

Observations of auroras are not only of academic interest, but are also a useful diagnostic tool for identifying zones of potentially dangerous geomagnetic disturbances [Vorobjev et al., 2018; Zou et al., 2022] due to the relationship of auroras with auroral electrojet. The auroral electrojet triggers the strongest geomagnetic disturbances on the Earth surface, but the strongest GIC bursts are associated with fast Pi3 pulsations (typical periods are the first tens of minutes) with high values of dB/dt [Pilipenko et al., 2024]. These pulsations are in fact a fine structure of the electrojet and can be accompanied by local intensification of auroras [Apatenkov et al., 2020].

In the Russian Federation, high-voltage PTLs are concentrated in the European part and extended eastward in the southern part (Figure 1). Since these PTLs, except for the Northern Transit line running along the Kola Peninsula, are located at lower geomagnetic latitudes than the auroral region, it would seem that magnetic storms do not pose a threat to the electric power system of the Russian Federation. However, during severe storms, the auroral oval boundaries and hence intense geomagnetic variations shift to the south. Can such storms pose a threat to the Russian electric power system, and if so, what is their intensity?

In this paper, we have constructed a map of risks for power and navigation systems in the Russian Federation, which are caused by severe storms and substorms in the night sector on the geomagnetic meridian of Moscow for extreme *Dst* and *AL* according to S93, ARM, APM_GEO, OP, and L2025. For space geophysics, comparing the results of different models is interesting because it allows us to figure out whether these models can be extrapolated to the case of extreme disturbances. The ultimate objective of the work is to outline approaches to real-time assessment of risks to man-made facilities in the territory of the Russian Federation that may arise during magnetic storms and substorms.

AURORAL OVAL MODELS

The S93 model

Starkov [1994] systematized locations of the equatorial boundary of auroras depending on the *AL* index and magnetic local time (MLT), using photographic observations at auroral latitudes obtained by various researchers. He also proposed formulas for determining auroral oval boundaries depending on the *AL* index, which characterizes the intensity of substorms. The empirical dependence of the lowest possible geomagnetic latitude of discrete auroras at the zenith in the near-

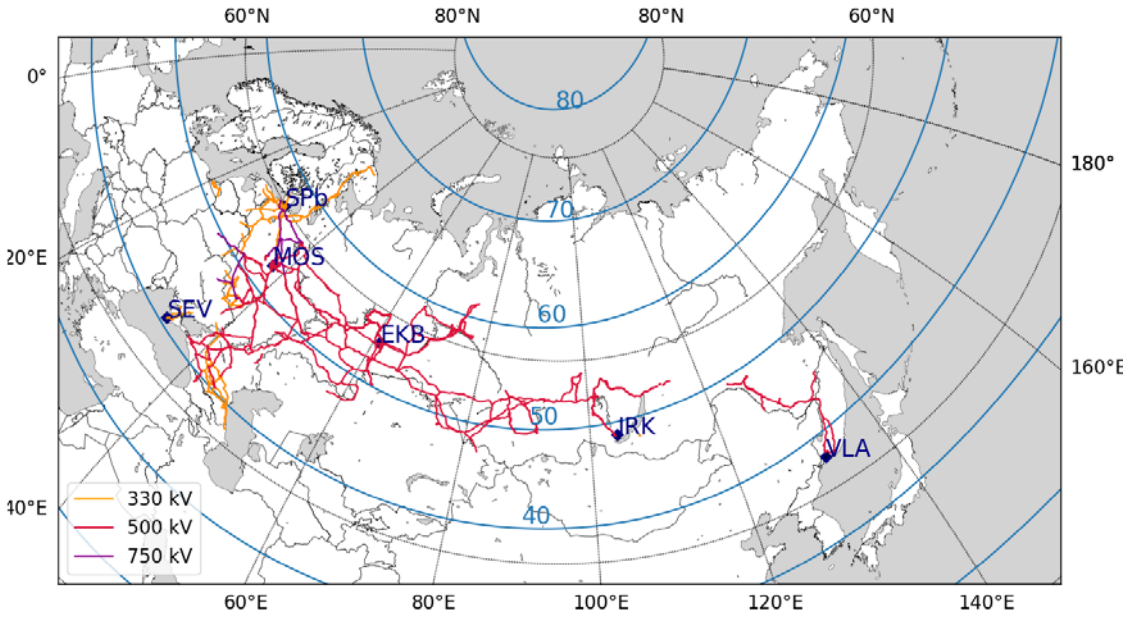

Figure 1. Map of the main power transmission lines of the Russian Federation with some industrial centers. Blue lines indicate geomagnetic latitudes; gray dotted lines, geographic latitudes. The magnetic coordinates are calculated by the AACGC model for an altitude of 100 km for May 10, 2024

midnight hours on magnetic storm intensity $\Phi(|Dst|)$ is approximated by the relation [Starkov, 1993]

$$\Phi = 74.9° - 8.6 \lg|Dst|. \quad (1)$$

This relation was further verified and confirmed in [Zverev et al., 2012].

The OVATION Prime model

A source of detailed and almost continuous information about the auroral oval structure is low-orbit satellite measurements of electron fluxes generating auroras. Satellite data on particle fluxes does not depend on illumination of the ionosphere and cloudiness, is available for both hemispheres, and is more reliable and accurate than ground or satellite optical observations of auroras. The auroral oval model OVATION Prime (OP) is based on more than twenty years of observations of electron and proton fluxes of different energies on DMSP satellites (altitude ~800 km). The OP model [Newell et al., 2010] can predict the energy flux, particle number flux, and average energy of precipitating electrons and ions at geomagnetic latitudes above 50°. The model is parameterized by solar wind and interplanetary magnetic field (IMF) parameters from the OMNI database and allows us to calculate with 1 hr resolution the expected two-dimensional spatial distribution of the intensity of auroral electron and ion precipitation of the main types [Newell et al., 2009]. The boundary of soft low-energy electron (0.1–10 keV) precipitation is taken as the boundary of discrete auroras. The OP model uses a previously established statistical relationship between interplanetary medium parameters and dynamics of auroral particle fluxes [Newell et al., 2007]. The OP model can predict the location and intensity of the auroral oval with ~1 hr horizon from real-time data obtained by satellites, located at the libration point.

The technical difficulty in applying this model to past events is associated with the fact that in order to compare simulation results with *Dst* it is necessary to have an empirical model of the relationship between interplanetary parameters and geomagnetic indices. Although these relationships have been determined statistically [Pallocchia et al., 2006; Boroyev et al., 2020], they are unknown for extreme events.

APM

The Auroral Precipitation Model (APM) [http://apm.pgia.ru/data] for auroral precipitation boundaries was constructed from DMSP F6 and F7 satellite data and was parameterized by the geomagnetic indices *Dst* and *AL*. The database contains the results of more than 30000 DMSP satellite passages in the Northern and Southern hemispheres in 1986. During this period, storms with $|Dst|<200$ nT and substorms with $|AL|<1500$ nT occurred. An important feature of APM is that the use of the two indices (although they are not completely independent) allows us to examine situations such as a magnetic storm without a substorm and a substorm without a magnetic storm. APM provides planetary distribution of boundaries of precipitation of different types in corrected geomagnetic (CGL-MLT) and geographic coordinates, as well as energy fluxes and the average energy of penetrating particles depending on geomagnetic activity level. Auroral regions with different characteristics of precipitating particles are classified as follows: DAZ (diffuse auroral zone) — a region of diffuse precipitation to the equator of the oval, which coincides with the zone of diffuse auroras; AOP (auroral oval precipitation) — a region of structured precipitation whose equatorial boundary coincides with the oval's equatorial boundary of discrete auroras; SDP (soft diffuse precipi-

tation to the pole of AOP [Vorobjev, Yagodkina, 2005]. During near-midnight hours, the electrojet equatorial boundary can be approximated fairly well by the location of the AOP equatorial boundary [Vorobjev et al., 2018]. Its geomagnetic latitude in the night sector (21–24 MLT) is approximated by the formula [Vorobjev, Yagodkina, 2007]

$$\Phi = 66.66 - 0.0092|AL| + 7.78\cdot10^{-7} AL^2 - \\ -0.022|Dst|. \quad (2)$$

Nonetheless, the approximations used in this model are limited to $|AL|<1500$ nT, and $|Dst|<200$ nT. At high $|AL|$, APM produces an unrealistic shape of the oval.

The new version APM_GEO, developed for the Northern Hemisphere [Vorobjev et al., 2023], is presented on the PGI website [https://pgia.ru/data/spaceweather/]. In APM_GEO, a fine regular MLT grid is set through interpolation by the Lagrange polynomial of initial values. Due to this detailed interpolation, APM_GEO is free from the disadvantage of the previous version — distortion of the oval shape in the dawn and dusk sectors at high *AL*. The model provides a distribution of flux intensities in precipitation zones for the given geomagnetic indices and allows us to calculate boundaries of precipitation zones in both geographic and geomagnetic coordinates. In APM_GEO, the limitations on the level of magnetic activity according to *AL* and *Dst* were removed, which makes it possible to roughly estimate the location and characteristics of precipitation during superstorms and extreme magnetic storms.

Empirical dependence of L2025

As we have already mentioned, Love et al. [2025] used eyewitness accounts of auroras published in journals and newspapers as a source of information about latitudes of auroras during extreme storms. Most of these accounts concerned the brightest discrete auroras observed at night. On this basis, a statistical model of the minimum latitude of the equatorial boundary of discrete auroras L2025 was constructed depending on the *Dst* index. The collected archive of observations contains magnetic storms with $|Dst|>200$ nT. In particular, the collection includes extreme storms and supersubstorms on September 2, 1859 ($|Dst|=964$ nT), February 4, 1872 ($|Dst|=801$ nT), May 15, 1921 ($|Dst|=907$ nT), etc. The regression relationship between $|Dst|$ and the parameter of the magnetic shell of the equatorial boundary of auroras *L* was determined as follows

$$\ln L = 3.9825 - 0.5478\ln|Dst|. \quad (3)$$

Variance of estimate (3) increases with $|Dst|$ due to the small number of extreme events.

Obviously, the L2025 model is not based on the most reliable data: there is no certainty that all observations relate to auroras at the zenith and in the night sector (21–24 MLT), the auroral oval emission may be confused with the red arc emission at lower latitudes, the geomagnetic indices are estimated very approximately for previous events, etc. The fundamental limitation of this model is that it does not explicitly highlight the role of auroral activity characterized by the *AL* index, which may affect the correctness of identification of the auroral oval equatorial boundary. Since the *AL* index is unknown for previous extreme magnetic storms, there are doubts that the latitude of observed aurora was defined only by *Dst*.

POSSIBLE LATITUDES OF AURORAL OVAL BOUNDARIES DEPENDING ON STORM INTENSITY

To compare L2025, APM, and S93, we have plotted the dependence of the geomagnetic latitude Φ ($|Dst|$) and the magnetic *L*-shell ($|Dst|$) for the night sector (21–24 MLT) (Figure 2). The parameter of the magnetic *L*-shell (the dimensionless distance to the top of the field line in Earth radii $r=LR_E$) was calculated from the ratio $\cos^2\Phi=(R_E+h)/LR_E$, where Φ is the geomagnetic latitude, $R_E=6370$ km, $h=250$ km — the height of the red auroral glow. For $R_E \gg h$ this yields the well-known relation $\cos\Phi = 1/\sqrt{L}$.

S93 and APM have limitations on the magnetic activity level, so we extrapolate dependences (1) and (2) to extreme storms up to $|Dst|\sim800$ nT. On the contrary, we extrapolate dependence (3), used in the L2025 model, to $|Dst|<200$ nT. In Figure 2, these portions of curves are indicated by strokes. APM approximation formula for the night sector (2) was used to estimate the auroral oval equatorial boundary during disturbances of the types “a storm without a substorm” ($|AL|=100$ nT), “a storm with a moderate substorm” ($|AL|=1000$ nT), and “a storm with a strong substorm” ($|AL|=1500$ nT). We are interested in whether the results of extrapolation of dependences (1) and (2) of S93 and APM for extreme geomagnetic disturbances are consistent with dependence (3) of L2025. For moderate storms ($|Dst|\sim200$ nT), APM gives $\Phi\sim55°$, which is close to $\Phi\sim54$ according to L2025. Latitudes $\Phi\sim54°$ correspond to the *L*-shell of ~3.2.

For more powerful storms, the dependences begin to diverge. For example, for a storm with $|Dst|=600$ nT, the discrepancy becomes significant: S93 and APM ($|AL|=100$ nT) yield $\Phi\sim52°$, whereas according to L2025 $\Phi\sim36°$. For extreme storms, the S93 model gives obviously unrealistic results, which is natural, since it is based on observations only in the auroral region. It suggests that extrapolations of the models based on observations of moderate storms (in this case, S93 and APM) cannot provide an objective assessment of the location of the auroral oval equatorial boundary during extreme storms. It would, however, be premature to say with certainty that the relationship between auroral oval location and storm intensity, established for moderate and severe storms, is violated for extreme storms, since the L2025 model cannot be considered reasonably valid.

Moreover, the APM curves for $|AL|=1000$ and 1500 nT (see Figure 2) indicate that it is impossible to correctly describe the auroral oval dynamics during storms without regard to the influence of substorms, since substorms lead

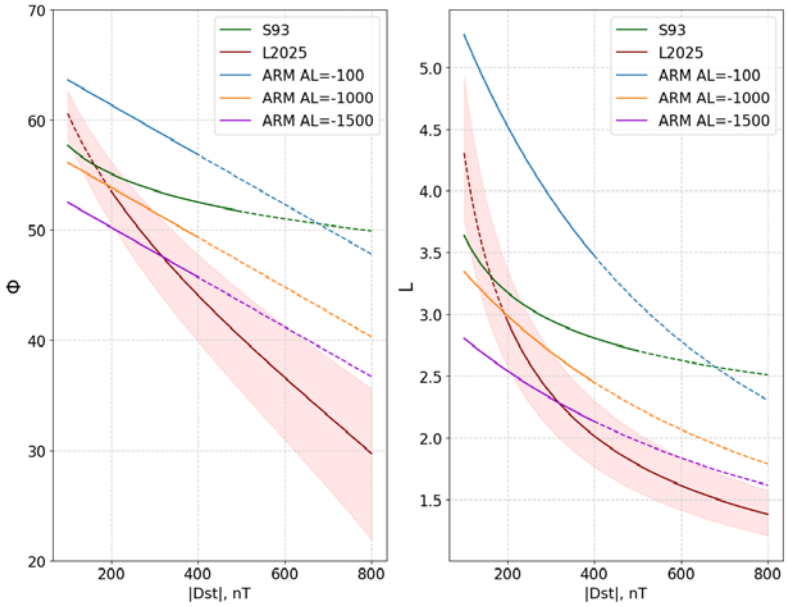

Figure 2. Geomagnetic latitude Φ (*a*) and *L*-shell (*b*) of the auroral oval equatorial boundary during near-midnight hours (MLT=21–24) as a function of |*Dst*| according to S93 (green line), L2025 (brown line), and APM for cases of storms without substorms (*AL*=–100 nT) (blue line) and with substorms *AL*=–1000 (orange line) and *AL*=–1500 nT (purple line). Strokes denote extrapolations outside the range of formal applicability of the models

City	Code	Geographic latitude	Geographic longitude	Geomagnetic latitude	Geomagnetic longitude	*L*-shell
Saint-Petersburg	SPB	59.9	30.3	56.1	107.0	3.3
Moscow	MOS	55.8	37.6	51.7	112.2	2.7
Ekaterinburg	EKB	56.9	60.6	52.7	133.9	2.8
Irkutsk	IRK	52.3	104.3	47.4	177.1	2.2
Sevastopol	SEV	44.6	33.5	39.7	106.3	1.7
Vladivostok	VLA	43.1	131.9	37.2	206.1	1.6

Calculated using [https://omniweb.gsf c.nasa.gov/vitmo/cgm.html], the epoch of 2000.

to a significant shift of the auroral oval equatorial boundary to the south.

In order to visualize the risk for different regions of the Russian Federation, Table presents geomagnetic coordinates of the main cities. The S93 model shows (see Figure 2) that during moderate storms with |*Dst*|~200 nT the auroral oval equatorial boundary reaches the latitude of Saint Petersburg (Φ~57°), and to the latitudes of Moscow and Ekaterinburg (Φ~52°–54°) it can shift only during a strong storm with |*Dst*|~400 nT. At the same time, the L2025 model predicts that during a storm with |*Dst*|~200 nT the auroral oval equatorial boundary will reach Saint Petersburg; with |*Dst*|~300 nT, Irkutsk (Φ~48°); and during an extreme storm with |*Dst*|~500 nT, Sevastopol (Φ~40°). Nonetheless, the combined effect of storms and substorms significantly changes the picture. As predicted by APM, the auroral oval will expand to midlatitudes even during relatively moderate (according to *Dst*) storms. So, at |*Dst*|~400 nT and |*AL*|~1500 nT, the auroral oval boundary will descend below Irkutsk to Φ~45°. During an extreme storm with |*Dst*|~600 nT, a substorm with |*AL*|~1500 nT can shift the auroral oval boundary to Φ~45° predicted by the L2025 model.

SPATIAL STRUCTURE OF THE OVAL

To assess whether particular regions of the Russian Federation are at risk during magnetic storms, we have mapped the auroral oval equatorial boundaries obtained from approximation formulas of S93 (Figure 3) and APM_GEO (Figure 4). The location of the boundaries was calculated for certain magnetic activity levels and for the time points corresponding to midnight on the meridian of Moscow (21 UT). Model geomagnetic latitudes were recalculated into geographic latitude, using the AACGM (Altitude Adjusted Corrected Geomagnetic Coordinates) model [Shepherd, 2014].

The S93 model can predict the location of the auroral oval boundary for different *AL*. Referring to Figure 3, at midnight during a strong substorm (|*AL*|=1000 nT) the equatorial boundary of the oval reaches Saint Petersburg, and during a supersubstorm (|*AL*|=2000 nT) it is located south of Moscow.

Figure 4 shows the location of the auroral oval equatorial boundary for a storm without a substorm at |*AL*|=100 nT and different |*Dst*| (200, 400, 600, and 800 nT) as calculated by APM_GEO. During moderate storms (|*Dst*|~200 nT), this boundary runs north of Saint

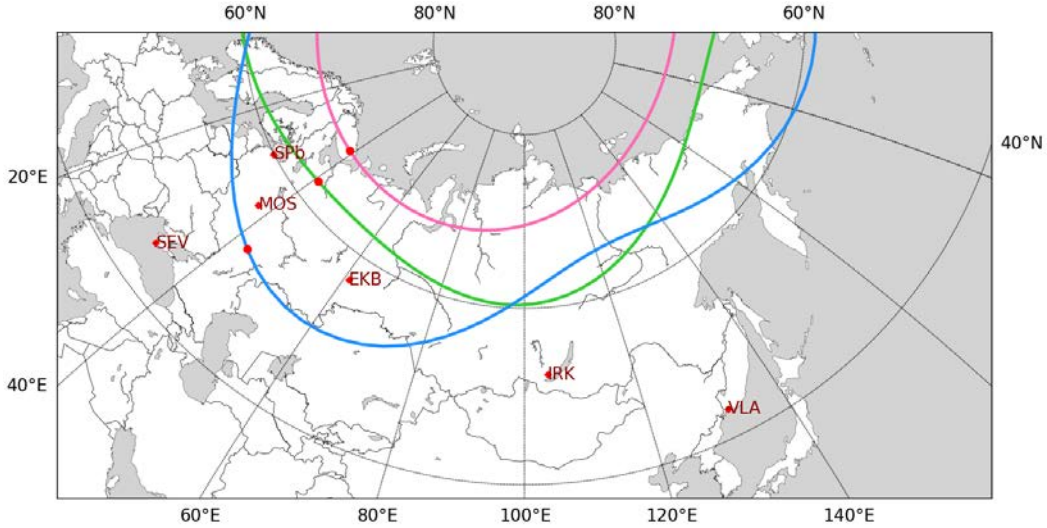

Figure 3. Geographic location of the auroral oval equatorial boundary for the territory of the Russian Federation for substorms of varying intensity according to the S93 model. Midnight on the meridian of Moscow is marked with red dots

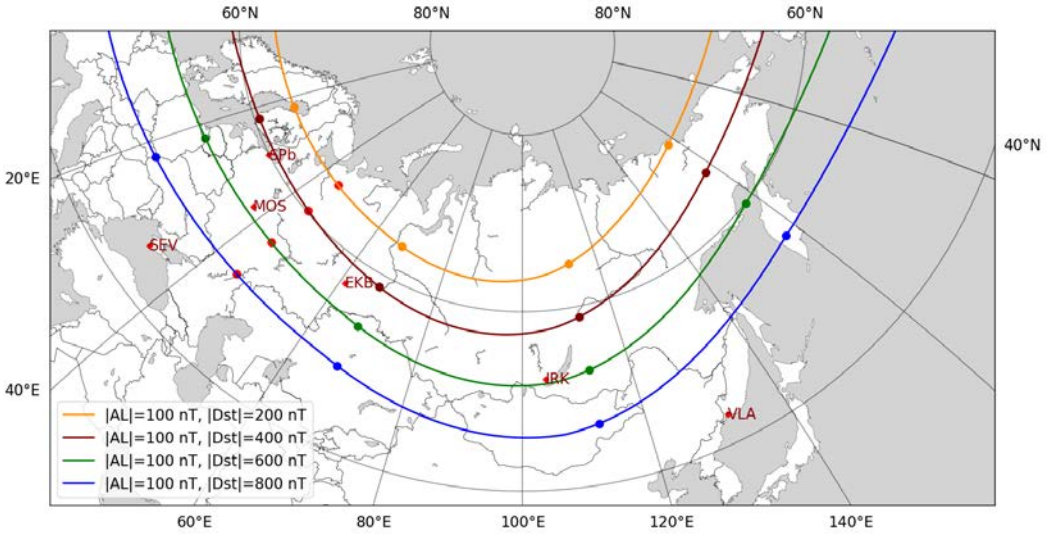

Figure 4. Geographic location of the auroral oval equatorial boundary for the territory of the Russian Federation according to APM_GEO for storms without substorms (|*AL*|=100 nT) with |*Dst*|=200, 400, 600, 800 nT. Dots on the curves mark centers of the sectors for which sets of coefficients are calculated; red dots indicate midnight on the meridian of Moscow

Petersburg, and during extreme storms (|*Dst*|~600 nT) it reaches Moscow and Irkutsk. Thus, according to APM_GEO, the region of the oval and probable GICs can cover a significant part of the territory of the Russian Federation only during very intense storms.

It is, however, impossible to build a unified picture of the location of the auroral oval equatorial boundary for magnetic storms due to possible occurrence of intense substorms (with high |*AL*|) during a storm. Locations of the auroral oval equatorial boundary according to APM_GEO for moderate storms with |*Dst*|=200 nT for substorms with |*AL*|=100, 1000, 2000 nT are depicted in Figure 5. In the absence of substorms, the auroral oval covers the Kola Peninsula and the White Sea. During a strong substorm (|*AL*|=1000 nT), the auroral oval equatorial boundary runs slightly north of Moscow and Ekaterinburg. During a supersubstorm (|*AL*|=2000 nT), the auroral oval equatorial boundary reaches the northern coast of the Caspian Sea.

Similarly, for the Far East located in the midnight sector of the auroral zone, during a moderate magnetic storm without strong substorms the auroral oval covers Chukotka (Figure 6). During a strong substorm (|*AL*|=1000 nT), the auroral oval equatorial boundary reaches Magadan. During a supersubstorm (|*AL*|=2000 nT), the auroral oval equatorial boundary extends to the southern tip of Kamchatka.

EFFECTS OF SUBSTORMS ON AURORAL OVAL DYNAMICS DURING A STORM

The fundamental problem in determining the location of the auroral oval equatorial boundary during magnetic storms, characterized by the *Dst* index, is the possibility of occurrence of intense substorms, which additionally affect the boundary location and increase the negative impact on man-made systems. In this regard, it is worthwhile examining two situations:

1) storms without substorms — the absence of substorms (|*AL*|<100 nT) during a storm;

2) high-intensity substorms (|*AL*|≥1000 nT) during a storm, in which the auroral oval equatorial boundary shifts considerably to low latitudes. This is particularly true for the night sector.

Since we are interested in the risks of failures in man-made facilities in industrial regions of the Russian Federation, we have evaluated the geomagnetic conditions under which these risks arise, using APM_GEO and L2025.

Figure 7 illustrates the dependence of the location of the auroral oval equatorial boundary Φ on *Dst* at |*AL*| from 500 to 2500 nT, which has been presented in [Vorobiev et al., 2025]. Locations of the auroral oval boundary according to the L2025 model have been added to these dependences. Along the Y-axis is the corrected geomagnetic latitude. During a moderate magnetic storm |*Dst*|~200 nT and a minor substorm |*AL*|~1000 nT, Saint Petersburg (Φ~57°) falls within the risk zone. If the substorm |*AL*| ~1000 nT becomes stronger, the risk zone covers Ekaterinburg (Φ~54°) and Moscow (Φ~52°). If a supersubstorm with |*AL*|~2500 nT develops during the storm, Irkutsk (Φ~48°) and Sevastopol (Φ~40°) are at risk. Thus, the same object may be at risk at different |*Dst*| values, depending on substorm intensity.

AURORAL OVAL BOUNDARIES FOR THE MAY 10–11, 2024 STORM

It is impossible to analyze predictions of the OP model for extreme storms, since the interplanetary medium parameters for those events are unknown. We will, therefore, consider the strongest magnetic storm in the first quarter of this century, on May 10–11, 2024, during which the *Dst* index was as high as –406 nT (on May 11 at 02 UT, Figure 8). During this event, the ionosphere was

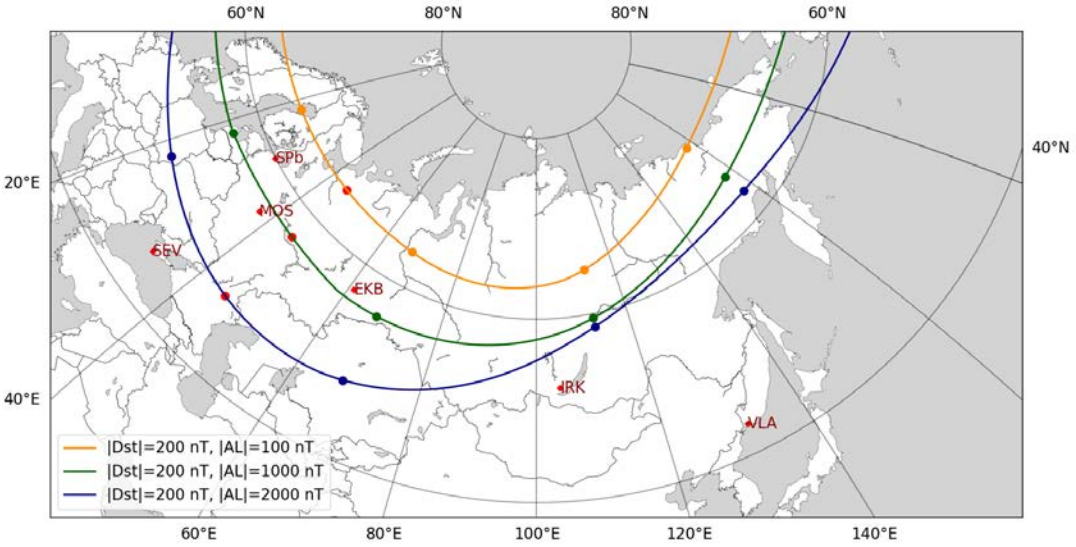

Figure 5. Geographic location of the auroral oval equatorial boundary for the Russian Federation according to APM_GEO for moderate storms (|*Dst*|=200 nT) with substorms of varying intensity (|*AL*|=100, 1000, 2000 nT) on the meridian of Moscow at midnight. Designations are the same as in Figure 4

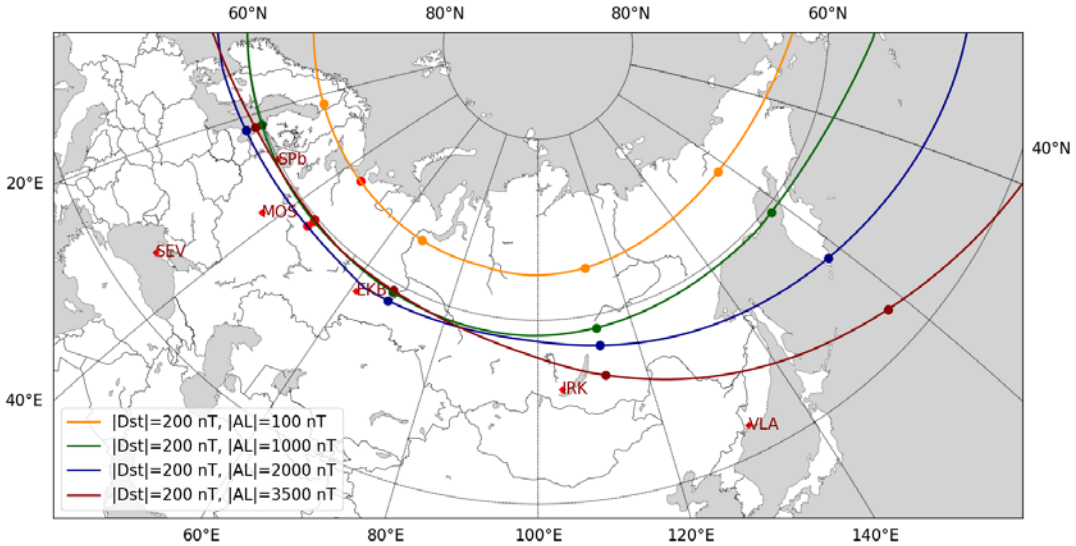

Figure 6. Geographic location of the auroral oval equatorial boundary for the Russian Federation according to APM_GEO for moderate storms (|*Dst*|=200 nT) with substorms of varying intensity (|*AL*|=100, 1000, 2000 nT) in the Far East at midnight. Designations are the same as in Figure 4

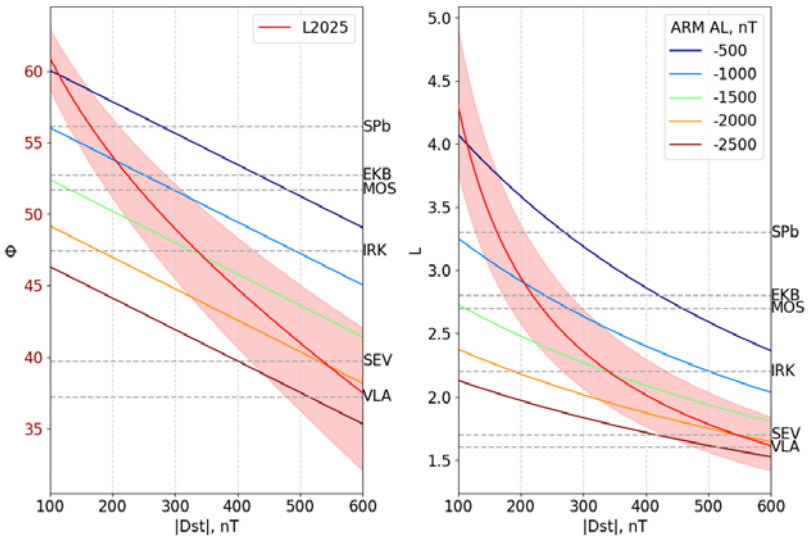

Figure 7. Corrected geomagnetic latitude of the auroral oval equatorial boundary Φ as function of *Dst* according to L2025 and APM at |*AL*| from 500 to 2500 nT for 21–24 MLT. Gray dashed lines denote latitudes of the selected cities of the Russian Federation

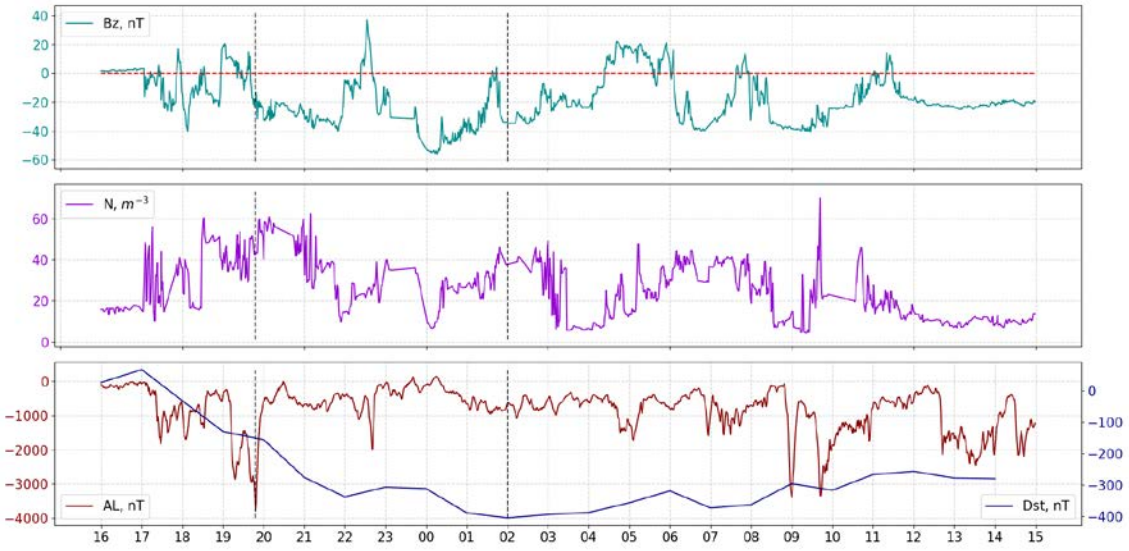

Figure 8. Variations in interplanetary medium parameters — IMF B_z (top panel) and solar wind density *N* (middle panel), as well as *AL* and *Dst* (bottom panel) during the storm from 16:00 UT on May 10, 2024 to 15:00 UT on May 11, 2024. The vertical dashed line marks the characteristic moments that are illustrated in Figure 9

strongly disturbed [Hiyadutuje et al., 2025], ~15–30 A GIC bursts were recorded on the Kola Peninsula in PTL Northern Transit in the night and dawn sectors [Despirak et al., 2025], and GIC bursts up to ~20 A were detected even in power grids of Central America [Caraballo et al., 2025].

From ~17 UT on May 10 to ~11 UT on May 11, 2024 on several long time intervals, IMF B_z was southward and ~40 nT (see Figure 8). This IMF orientation was favorable for constant influx of energy into the magnetosphere, which fed the storm with *Dst* of the order of several hundred nT. Variations in the geomagnetic indices and interplanetary medium parameters according to OMNI data suggest that two supersubstorms with |*AL*|>3000 nT occurred during the storm (indicated in Figure 8 by vertical dashed lines) [Gonzalez et al., 2011]. During the supersubstorms, there were no abrupt changes in the solar wind and IMF parameters. Thus, the substorms developed spontaneously and, due to the high energy pumped into the magnetosphere, reached a high intensity.

Let us compare the spatial structure of the oval obtained by APM_GEO and the OP model for several peculiar moments in the development of this storm. This comparison will demonstrate the relative contribution of the substorms to the storm. A supersubstorm during the growth phase of the storm was observed on May 10, 2024 at 19:48 UT with *Dst*=–157 nT and *AL*=–3797 nT. The OP model illustrates the distribution of the energy flux of precipitating electrons within auroral oval boundaries derived from the interplanetary medium parameters. According to this model, the auroral oval equatorial boundary only reaches Saint Petersburg (Figure 9, top panel). At the same time, according to APM_GEO, all major cities, except for Vladivostok, are at risk. For May 11, 2024 at 02:00 UT when *Dst* reached

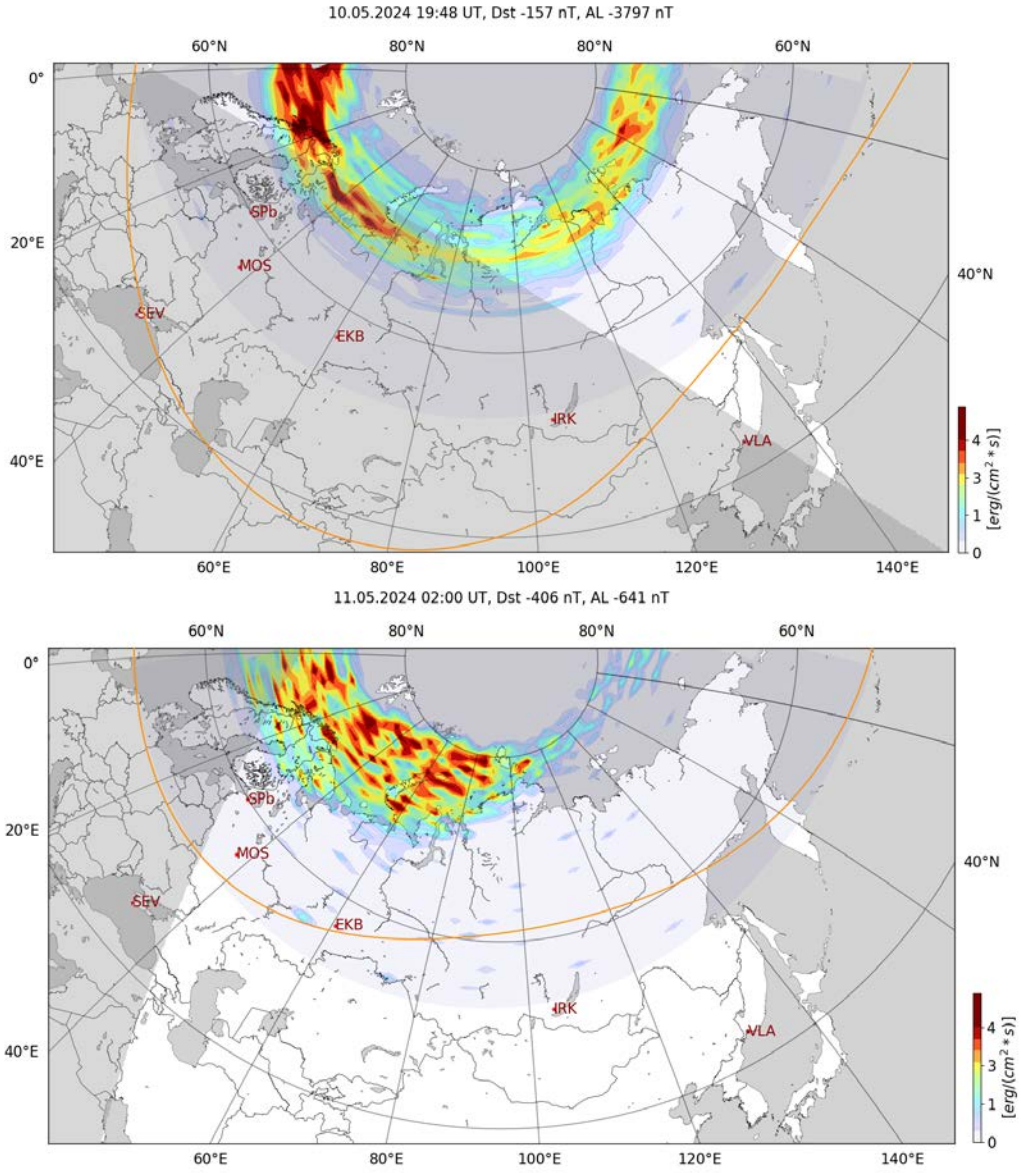

Figure 9. Comparison of the spatial pattern of the auroral oval over the Russian Federation according to the OP model and the auroral oval equatorial boundary according to APM_GEO (yellow line) for the characteristic moments of the May 10–11, 2024 magnetic storm: in the top panel is the supersubstorm during the growth phase of the magnetic storm on May 10, 2024 at 19:48 UT with *Dst*=–157 nT, *AL*=–3797 nT; in the bottom panel is the maximum of the magnetic storm on May 11, 2024 at 02:00 UT with *Dst*=–406 nT, *AL*=–641 nT. The pale ring on the map is defined by the non-zero background of the OP model

an extreme value of –406 nT and *AL*=–641 nT (see Figure 8), the OP model gives approximately the same picture of auroral oval location (see Figure 9, bottom panel), whereas APM_GEO shows that the auroral oval equatorial boundary extends to Ekaterinburg. In this situation, the location of auroral oval boundaries is generally determined by *Dst*. At high *Dst*, the oval expands in the dawn–dusk direction [Yagodkina et al., 2012], which we do observe, but the OP model cannot reproduce this feature.

During the recovery phase of the storm on May 11, 2024 at 09:00 UT, the epicenter of the substorm was over North America and Greenland; we do not analyze this here.

Thus, the OP model, controlled only by interplanetary medium parameters, does not reproduce the response of the auroral oval to spontaneously developing substorms and gives its strongly averaged location compared to APM_GEO.

DISCUSSION

Based on statistical analysis of data covering solar cycles 14–24, it has been estimated that a once-in-a-century storm has an intensity of the order of |*Dst*|=663 nT [Pulkkinen et al., 2012; Love, 2021]. According to the L2025 model, a storm of this intensity will cause discrete auroras up to the geomagnetic latitude of 34° and put electric power grids throughout the United States and Europe at risk. For the most powerful storm on record, the Carrington event on September 2, 1859 (*Dst*=–964 nT), according to the L2025 model the equatorial boundary should have been

at a geomagnetic latitude of ~24°, which would have caused a high level of GIC in power grids of Japan and most of China. In the Russian Federation, during such storms, GNSS failures will obviously occur in most heavily populated areas, and the entire Russian power system will be affected by GICs.

The intensity of magnetic storms is measured by the *Dst* index, which has a clear physical meaning. The Dessler—Parker—Skopke relation [Mazur, Shukhman 2015] relates the magnetic field disturbance ΔB~*Dst* in the center of the system to the total kinetic energy W_K of ring current particles:

$$\frac{\Delta B}{B_E} = \frac{2}{3}\frac{W_K}{W_B}, \quad (5)$$

where W_B is the total energy of the magnetic field in the system; B_E is the dipole magnetic field strength in the center of the system. Since *Dst* increases linearly with energy, it follows from (5) that the unusually high energy of ring current particles trapped by the magnetosphere is intrinsic to extreme magnetic storms. The dynamics of the auroral oval during storms should be closely linked to the dynamics of the main magnetospheric structures [Khorosheva, 1987]. The maximum intensity of radiation belt relativistic electrons L_{max} is related to the storm intensity by the ratio $L_{max} = 12.9/\sqrt[4]{|Dst|}$ [Tverskaya, 2011], i.e. L_{max}~2.9 for a storm with *Dst*=–400 nT.

If we accept the predictions of the L2025 model, compression of the magnetosphere during extreme storms does not reach the expected saturation. Thus, according to L2025, the auroral oval boundary drastically shifts to low latitudes with increasing disturbance and reaches *L*~1.5 at |*Dst*|~700 nT (see Figure 2). It is difficult to imagine what happens to the location of the main magnetospheric structures — the ring current, the radiation belt, etc. Apparently, it is somewhat premature to consider such a scenario, since the L2025 model is not based on the most reliable data and there is no certainty that all observations relate to auroras at the zenith and in the night sector. Moreover, the substorm dynamics during extreme storms is unknown, and there are doubts that the latitude of observed auroras was determined only by *Dst*. Estimates of the geomagnetic indices for historical extreme storms are also very uncertain. In general, there is often a situation where, according to eyewitnesses, auroras even during moderate magnetic storms were observed up to very low latitudes and much further south than all existing auroral oval models predict [Spogli et al., 2024]. In all likelihood, observers mistook the red arc at lower latitudes for the auroral oval.

Extrapolations of the S93 model and APM_GEO give a significantly lower effect of the southward shift of the auroral oval during extreme storms compared to the L2025 model, hence the size of the territories that may be threatened with GIC excitation is also much smaller. However, the development of intense substorms during the evolution of a storm may cause, according to APM_GEO, an additional shift of the auroral oval equatorial boundary and hence the electrojet to midlatitudes and significantly increase the area of negative impact on man-made systems.

Models are developed for real-time prediction of dynamics of the auroral oval during changes in space weather [Machol et al., 2012]. The empirical OP model, which can calculate the relationship between the intensity of auroral precipitation and the probability of their occurrence, is used on the NOAA web service [https://www.swpc.noaa.gov/products/aurora-30-minute-forecast], which provides real-time, 30-min forecasts of auroras. A web service for visualizing the probability of auroras has also been developed using the OP model with the help of geographic information systems [Vorobev et al., 2020a, b]. The input parameters of these models are NASA's real-time data on the solar wind and IMF from satellites located at the libration point. The time shift (~1 hr) due to propagation of the solar wind from the libration point L1, near which the satellite is located, to the boundary of the magnetosphere allows us to make a short-term forecast of the expected intensity of auroras around the globe. The same models can seemingly be used to predict the location of spatial zones with possible strong GICs, yet there are several circumstances that significantly complicate the solution of this problem.

Although the GIC strength increases on average with increasing intensity of auroras, there is no simple linear relationship between them, since the most intense GIC bursts are caused by local eddy current structures against the background of auroral electrojet, and these structures may be associated with local brightenings of auroras [Engebretson et al., 2019; Apatenkov et al., 2020]. Thus, the proximity of the auroral oval and electrojet to a technological system is a necessary but insufficient condition for the occurrence of strong GICs. Furthermore, the greatest geomagnetic disturbances and shifts of the auroral oval and electrojet to the south during a storm are associated with substorms whose occurrence the OP model cannot predict. As a result, the OP model gives a very average location of the oval and considerably underestimates its shift to the south.

CONCLUSION

If we consider the auroral oval as an indicator of the location of electrojet, information about the location of the oval allows us to predict at which latitudes the most intense geomagnetic variations, which generate dangerous GICs in electric power grids, can be observed. The S93, OP models, and APM are widely employed to predict the location of the oval during moderate and strong storms and substorms. To construct the statistical model of the minimum latitude of the equatorial boundary of discrete auroras L2025, Love et al. [2025] used published information on visual observations of auroras during extreme storms. Our comparison of dependences of the latitude of auroras on storm intensity, obtained by extrapolating S93 and APM, with L2025 predictions has revealed that the patterns of the relationship between the oval and storm intensity, established for moderate and strong storms (|*Dst*|<400 nT), are violated during extreme storms (|*Dst*|>400 nT). Using the May 10–11, 2024 extreme storm as an example, it is shown that the OP model gives a very average location of the oval and significantly underestimates its shift to the south. This is

due to the fact that the most considerable geomagnetic disturbances and shifts of the auroral oval and electrojet during a storm are linked to spontaneously developing supersubstorms whose occurrence the OP model cannot predict. To assess the possible risks posed by GICs, it is necessary to test maps of the auroral oval equatorial boundary for the Russian Federation for probable *Dst* and *AL* obtained by different models. Using such a map presented in this paper as example, we have shown that according to APM_GEO a sharp descent of the auroral oval equatorial boundary occurs during substorms developing during storms. As a result, in view of the combined effect of storms and substorms, all large electric power grids of the Russian Federation are affected by GICs, and at midlatitudes GNSS failures may occur not only during extreme magnetic storms, but also during strong ones.

We express our gratitude to V.G. Vorobjev for useful discussions and O.V. Mingalev for his assistance with APM_GEO calculations.

The work was financially supported by RSF (grant No. 21-77-30010-P).

REFERENCES

Apatenkov S.V., Pilipenko V.A., Gordeev E.I., et al. Auroral omega bands are a significant cause of large geomagnetically induced currents. *Geophys. Res. Lett.* 2020, vol. 47, e2019GL086677. https://doi.org/10.1029/2019GL086677.

Baker D.N., Balstad R., Bodeau J.M., et al. Severe space weather events — Understanding societal and economic impacts. The National Academy Press, Washington, 2008. https://doi.org/10.17226/12507.

Blake S.P., Pulkkinen A., Schuck P.W., et al. Estimating maximum extent of auroral equatorward boundary using historical and simulated surface magnetic field data. *J. Geophys. Res.* 2021, vol. 126, iss. 2, e2020JA028284. https://doi.org/10.1029/2020JA028284.

Boroyev R.N., Vasiliev M.S., Baishev D.G. The relationship between geomagnetic indices and the interplanetary medium parameters in magnetic storm main phases during CIR and ICME events. *J. Atmos. Sol.-Terr. Phys.* 2020, vol. 204, 105290. https://doi.org/10.1016/j.jastp.2020.105290.

Boteler D.H. Geomagnetic hazards to conducting networks. *Natural Hazards*. 2003, vol. 28, iss. 2, pp. 537–561. https://doi.org/10.1023/A:1022902713136.

Caraballo R., Gonzalez-Esparza J.A., Pacheco C.R., et al. The impact of geomagnetically induced currents (GIC) on the Mexican power grid: Numerical modeling and observations from the 10 May 2024 geomagnetic storm. *Geophys. Res. Lett.* 2025, vol. 52, iss. 4, e2024GL112749. https://doi.org/10.1029/2024GL112749.

Carbary J.F., Sotirelis T., Newell P.T., Meng C.-I. Auroral boundary correlations between UVI and DMSP. *J. Geophys. Res.* 2003, vol. 108, iss. A1, pp. SIA2-1–SIA2-7. 10.1029/2002JA009378.

Chisham G., Burrell A.G., Thomas E.G., Chen Y.-J. Ionospheric boundaries derived from auroral images. *J. Geophys. Res.* 2022, vol. 127, iss. 7, e2022JA030622. https://doi.org/10.1029/2022JA03062.

Despirak I., Setsko P., Lubchich A., et al. Geomagnetically induced currents (GICs) during strong geomagnetic storm on 10–12 May 2024. *Adv. Space Res.* 2025. https://doi.org/10.1016/j.asr.2025.06.081.

Dimmock A.P., Rosenqvist L., Hall J.-O., et al. The GIC and geomagnetic response over Fennoscandia to the 7–8 September 2017 geomagnetic storm. *Space Weather*. 2019, vol. 17, iss. 7, pp. 989–1010. https://doi.org/10.1029/2018SW002132.

Edemskiy I.K., Yasyukevich Yu.V. Auroral oval boundary dynamics on the nature of geomagnetic storm. *Remote Sens.* 2022, vol. 14, 5486. https://doi.org/10.3390/rs14215486.

Effects of Space Weather on Technology Infrastructure. Kluwer Academic Publishers, 2004, 343 p. https://doi.org/10.1007/1-4020-2754-0.

Engebretson M.J., Steinmetz E.S., Posch J.L., et al. Nighttime magnetic perturbation events observed in Arctic Canada: 2. Multiple-instrument observations. *J. Geophys. Res.* 2019, vol. 124, pp. 7459–7476. https://doi.org/10.1029/2019JA026797.

Evdokimova M.A., Petrukovich A.A. Estimation of westward auroral electrojet current with magnetometer chain data. *Ann. Geophys.* 2020, vol. 38, pp. 109–121. https://doi.org/10.5194/angeo-38-109-2020.

Feldstein Ya.I. Some issues of the morphology of auroras and magnetic disturbances at high latitudes. *Geomagnetism and Aeronomy*. 1963, vol. 3, iss. 2, pp. 227–239. (In Russian).

Feldstein Y.I., Gromova L.I., Grafe A., et al. Dynamics of the auroral electrojets and their mapping to the magnetosphere. *Radiation Measurements*. 1999, vol. 30, iss. 5, pp. 579–587. https://doi.org/10.1016/S1350-4487(99)00219-X.

Gary J.B., Zanetti L.J., Anderson B.J., et al. Identification of auroral oval boundaries from in situ magnetic field measurements. *J. Geophys. Res.* 1998, vol. 103, iss. A3, pp. 4187–4197. https://doi.org/10.1029/97JA02395.

Gonzalez W.D., Echer E., Tsurutani B.T., et al. Interplanetary origin of intense, superintensive and extreme geomagnetic storms. *Space Sci. Rev*. 2011, vol. 158, iss. 1, pp. 69–89. https://doi.org/10.1007/s11214-010-9715-2.

Gvishiani A.D., Lukyanova R.Yu. Estimating the influence of geomagnetic disturbances on the trajectory of the directional drilling of deep wells in the Arctic region. *Izvestiya, Physics of the Solid Earth*. 2018, vol. 54, iss. 4, pp. 554–564. https://doi.org/10.1134/S1069351318040055.

Hapgood M.A. Prepare for the coming space weather storm. *Nature*. 2012, vol. 484, pp. 311–313. https://doi.org/10.1038/484311.

Hiyadutuje A., Bilitza D., Ojebisi T., et al. Assessment of the performance of the IRI's auroral oval boundary model as applied to the Mother's Day G5 storm during 10–13 May 2024. *Adv. Space Res*. 2025, vol. 76, iss. 12, pp. 7241–7250. https://doi.org/10.1016/j.asr.2025.04.003.

Johnsen M.G. Real-time determination and monitoring of the auroral electrojet boundaries. *J. Space Weather Space Climate*. 2013, vol. 3, A28. https://doi.org/10.1051/swsc/2013050.

Kataoka R., Ngwira C. Extreme geomagnetically induced currents. *Progress in Earth and Planetary Science*. 2016, vol. 3, 23. https://doi.org/10.1186/s40645-016-0101-x.

Khorosheva O.V. Spatio-temporal distribution of polar auroras and their relationship with high-latitude geomagnetic disturbances. *Geomagnetism and Aeronomy*. 1961, vol. 1, iss. 5, pp. 695–701. (In Russian).

Khorosheva O.V. Magnetospheric disturbances and the associated dynamics of ionospheric electrojets, polar auroras and plasmapause. *Geomagnetism and Aeronomy*, 1987, vol. 27, iss. 5, pp. 804–811. (In Russian).

Kostarev D.V., Pilipenko V.A., Kozyreva O.V. Geomagnetic monitoring to mitigate risk to pipelines from space weather. *Science & Technologies: Oil and Oil Products Pipeline Transportation*. 2023, vol. 13, iss. 1, pp. 38–49. (In Russian). https://doi.org/10.28999/2541-9595-2023-13-1-38-49.

Kozyreva O.V., Pilipenko V.A., Engebretson M.J., et al. Correspondence between the ULF wave power distribution and auroral oval. *Sol.-Terr. Phys.* 2016, vol. 2, iss. 2, pp. 46–65. https://doi.org/10.12737/20999.

Kozyreva O., Pilipenko V., Belakhovsky V., Sakharov Ya. Ground geomagnetic field and GIC response to March 17, 2015, storm. *Earth, Planets and Space.* 2018, vol. 70, 157. https://doi.org/10.1186/s40623-018-0933-2.

Love J.J. Extreme-event magnetic storm probabilities derived from rank statistics of historical *Dst* intensities for solar cycles 14–24. *Space Weather.* 2021, vol. 19, iss. 4, e2020SW002579. https://doi.org/10.1029/2020SW002579.

Love J.J. Mann I.R., Qvick T., Mursula K. What is the lowest latitude of discrete aurorae during superstorms? *Space Weather*. 2025, vol. 23, e2024SW004286. https://doi.org/10.1029/2024SW004286.

Machol J.L., Green J.C., Redmon R.J., et al. Evaluation of OVATION prime as a forecast model for visible aurorae. *Space Weather*. 2012, vol. 10, S03005. https://doi.org/10.1029/2011SW000746.

Mazur V.A., Shukhman I.G. On the derivation of Dessler—Parker—Sckopke relation. *Sol.-Terr. Phys.* 2015. vol. 1, iss. 2, pp. 80–84. (In Russian). https://doi.org/10.12737/7495.

Myagkova I.M., Ryazantseva M.O., Antonova E.E., Marjin B.V. Enhancements of fluxes of precipitating energetic electrons on the boundary of the outer radiation belt of the Earth and position of the auroral oval boundaries. *Space Res.* 2010, vol. 48, pp. 165–173. https://doi.org/10.1134/S0010952510020061.

Newell P.T., Sotirelis T., Liou K., et al. A nearly universal solar wind-magnetosphere coupling function inferred from 10 magnetospheric state variables. *J. Geophys. Res.* 2007, vol. 112, A01206. https://doi.org/10.1029/2006JA012015.

Newell P.T., Sotirelis T., Wing S. Diffuse, monoenergetic, and broadband aurora: The global precipitation budget. *J. Geophys. Res.* 2009, vol. 114, A09207. https://doi.org/10.1029/2009JA014326.

Newell P.T., Sotirelis T., Wing S. Seasonal variations in diffuse, monoenergetic, and broadband aurora. *J. Geophys. Res.* 2010, vol. 115, A03216. https://doi.org/10.1029/2009JA014805.

Newell P.T., Liou K., Zhang Y., et al. OVATION Prime-2013: Extension of auroral precipitation model to higher disturbance levels. *Space Weather*. 2014, vol. 12, pp. 368–379. https://doi.org/10.1002/2014SW001056.

Pallocchia G., Amata E., Consolini G., et al. Geomagnetic Dst index forecast based on IMF data only. *Ann. Geophys.* 2006, vol. 24, pp. 989–999. https://doi.org/10.5194/angeo-24-989-2006.

Pilipenko V., Yagova N., Romanova N., Allen J. Statistical relationships between the satellite anomalies at geostationary orbits and high-energy particles. *Adv. Space Res.* 2006, vol. 37, iss. 6, pp. 1192–1205. https://doi.org/10.1016/j.asr.2005.03.152.

Pilipenko V.A. Impact of space weather on ground-based technological systems. *Sol.-Terr. Phys.* 2021, vol. 7, iss. 3, pp. 68–104. https://doi.org/10.12737/stp-73202106.

Pilipenko V.A., Chernikov A.A., Soloviev A.A., et al. Influence of space weather on the reliability of the transport system functioning at high latitudes. *Russian Journal of Earth Sciences*. 2023a, vol. 23, no. 2, ES2008. (In Russian). https://doi.org/10.2205//2023ES000824.

Pilipenko V.A., Gvishiani A.D., Soloviev A.A., Rosenberg I.N. Space weather and railways. *Earth and the Universe*. 2023b, iss. 6, pp. 22–34. (In Russian). https://doi.org/10.7868/S0044394823060026.

Pilipenko V.A., Kozyreva O.V., Belakhovsky V.B., et al. What should we know to predict geomagnetically induced currents in power transmission lines? *Russian Journal of Earth Sciences.* 2024, vol. 24, ES6006. https://doi.org/10.2205/2024es000954.

Pulkkinen A., Bernabeu E., Eichner J., et al. Generation of 100-year geomagnetically induced current scenarios. *Space Weather*, 2012, vol. 10, iss. 4, S04003. https://doi.org/10.1029/2011SW000750.

Shepherd S.G. Altitude-adjusted corrected geomagnetic coordinates: Definition and functional approximations. *J. Geophys. Res.* 2014, vol. 119, pp. 7501–7521. https://doi.org/10.1002/2014JA020264.

Sotirelis T., Newell P.T. Boundary-oriented electron precipitation model. *J. Geophys. Res*. 2000, vol. 105, iss. A8, pp. 18655–18673. https://doi.org/10.1029/1999JA000269.

Spogli L., Alberti T., Bagiacchi P., et al. The effects of the May 2024 Mother's Day superstorm over the Mediterranean sector: from data to public communication. *Ann. Geophys.* 2024, vol. 67, iss. 2, PA218. https://doi.org/10.4401/ag-9117.

Starkov G.V. Planetary morphology of auroras. *Magnetospheric-Ionospheric Physics. Brief Handbook.* St. Petersburg, Nauka Publ., 1993, pp. 85–90. (In Russian).

Starkov G.V. Mathematical description of the auroral oval boundaries. *Geomagnetism and Aeronomy*. 1994, vol. 34, iss. 3, pp. 80–86. (In Russian).

Tverskaya L.V. Diagnostics of the magnetosphere based on the outer belt relativistic electrons and penetration of solar protons: A review. *Geomagnetism and Aeronomy*. 2011, vol. 51, iss. 1, pp. 6–22. https://doi.org/10.1134/S0016793211010142.

Vorobjev V.G., Yagodkina O.I. Effect of magnetic activity on the global distribution of auroral precipitation zone. *Geomagnetism and Aeronomy*. 2005, vol. 45, iss. 4, pp. 438–444. (In Russian).

Vorobjev V.G., Yagodkina O.I. Auroral precipitation dynamics during strong magnetic storms. *Geomagnetism and Aeronomy*. 2007, vol. 47, iss. 2, pp. 185–192. https://doi.org/10.1134/S0016793207020065.

Vorobjev V.G., Yagodkina O.I., Katkalov Y. Auroral precipitation model and its applications to ionospheric and magnetospheric studies. *J. Atmos. Sol.-Terr. Phys.* 2013, vol. 102, pp. 157–171. https://doi.org/10.1016/j.jastp.2013.05.007.

Vorobjev V.G., Sakharov Ya.A., Yagodkina O.I., et al. Geomagnetically induced currents and their relationship with locations of westward electrojet and auroral precipitation boundaries. *Transactions of the Kola Science Center of the Russian Academy of Sciences*. 2018, vol. 5, iss. 4, pp. 16–28. (In Russian). https://doi.org/10.25702/KSC.2307-5252.2018.9.5.16-28.

Vorobev A.V., Pilipenko V.A., Krasnoperov R.I., et al. Short-term forecast of the auroral oval position on the basis of the "virtual globe" technology. *Russian J. Earth Science*. 2020a, vol. 20, ES6001. https://doi.org/10.2205/2020ES000721.

Vorobev A.V., Pilipenko V.A., Reshetnikov A.G., et al. Web-oriented visualization of auroral oval geophysical parameters. *Scientific Visualization*. 2020b, vol. 12, no. 3, pp. 108–118. https://doi.org/10.26583/sv.12.3.10.

Vorobjev V.G., Yagodkina O.I., Melnik M.N., Mingalev O.V. Planetary distribution of characteristics of electron and ion precipitation depending on the levels of magnetic activity. Interactive model APM_GEO. *Physics of Auroral Phenomena. Proc. XLVI Annual Seminar.* Apatity, 2023, pp. 127–136. (In Russian). https://doi.org/10.51981/2588-0039.2023.46.028.

Vorobiev V.G., Yagodkina O.I., Antonova E.E. Nightside auroral precipitations under extreme levels of geomagnetic activity. *Physics of Auroral Phenomena. Proc. XLVIII Annual Seminar*. Apatity, 2025, pp. 54–58. (In Russian). https://doi.org/10.51981/2588-0039.2025.48.012.

Walker S.J., Laundal K.M., Reistad J.P., et al. A comparison of auroral oval proxies with the boundaries of the auroral electrojets. *Space Weather*. 2024, vol. 22, iss. 4, e2023SW003689. https://doi.org/10.1029/2023SW003689.

Woodroffe J.R., Morley S.K., Jordanova V.K., et al. The latitudinal variation of geoelectromagnetic disturbances during large (*Dst*≤–100 nT) geomagnetic storms. *Space Weather*. 2016, vol. 14, iss. 9, pp. 668–681. https://doi.org/10.1002/2016SW001376.

Xiong C., Lühr H., Wang H., Johnsen M.G. Determining the boundaries of the auroral oval from CHAMP field-aligned current signatures — Part 1. *Ann. Geophys.* 2014, vol. 32, iss. 6, pp. 609–622. https://doi.org/10.5194/angeo-32-609-2014.

Yagodkina O.I., Despirak I.V., Vorobjev V.G. Spatial distribution of auroral precipitation during storms caused by magnetic clouds. *J. Atmos. Sol.-Terr. Phys.* 2012, vol. 77, pp. 1–18. https://doi.org/10.1016/j.jastp.2011.06.009.

Yasyukevich Yu.V., Edemskiy I.K., Perevalova N.P., Polyakova A.S. *Response of the Ionosphere to Helio- and Geophysical Disturbances According to GPS Data*. Irkutsk, Irkutsk State University Publ., 2013. 259 p. (In Russian).

Zou Y., Dowell C., Ferdousi B., et al. Auroral drivers of large dB/dt during geomagnetic storms. *Space Weather*. 2022, vol. 20, iss. 11, e2022SW003121. https://doi.org/10.1029/2022SW003121.

Zverev V.L., Feldshtein Ya.I., Vorobjev V.G. Auroral glow to the equator from the polar auroral oval. *Geomagnetism and Aeronomy*. 2012, vol. 52, iss. 1, pp. 60–67. https://doi.org/10.1134/S0016793212010173.

URL: http://apm.pgia.ru/data (accessed December 12, 2025).

URL: https://pgia.ru/data/spaceweather/ (accessed December 12, 2025).

URL: https://omniweb.gsfc.nasa.gov/vitmo/cgm.html (accessed December 12, 2025).

URL: https://www.swpc.noaa.gov/products/aurora-30-minute-forecast (accessed December 12, 2025).

Original Russian version: Savelyeva N.V., Pilipenko V.A., Yagodkina O.I., published in Solnechno-zemnaya fizika. 2026, vol. 12, no. 2, pp. 24–37. DOI: https://doi.org/10.12737/szf-122202603.

How to cite this article

Savelyeva N.V., Pilipenko V.A., Yagodkina O.I. Which latitudes of the Russian Federation may be affected by extreme magnetic storms? *Sol.-Terr. Phys.* 2026, vol. 12, iss. 2, pp. 21–33. https://doi.org/10.12737/stp-122202603.